

Dehydrogenation-induced polarity flipping of charge carriers and conductance enhancement in nitrogen-containing heterocyclic molecule-anchored single-molecule junctions

Qi Zhou(周琦), Ruimei Liu(刘瑞梅), Guang-Ping Zhang(张广平), Chuan-Kui Wang(王传奎), and Minglang Wang(王明郎)

Citation: Chin. Phys. B, 2026, 35 (**7**): 077301. DOI: 10.1088/1674-1056/ae0d56
http://cpb.iphy.ac.cn; http://iopscience.iop.org/cpb

What follows is a list of articles you may be interested in

Ultra-high anisotropy and electronic property of two-dimensional $PbSnS_2$ with a black phosphorus structure

Xinlong Wang(王鑫龙), Shihao Wang(王诗皓), Yandi Jiang(姜彦迪), Qing Min(闵清), Haiming Huang(黄海铭), Chengrui Wu(吴承瑞), and Juntao Yang(杨俊涛)
Chin. Phys. B, 2026, 35 (**5**): 057304. DOI: 10.1088/1674-1056/ae1568

Improve thermoelectric properties of graphene nanoribbons based on resonant structure engineering

Yu-Xuan Kang(康宇轩), Shi-Yun Xiong(熊世云), and Hong-Liang Yi(易红亮)
Chin. Phys. B, 2026, 35 (**3**): 037301. DOI: 10.1088/1674-1056/ae1950

Quantum confinement of carriers in the type-I quantum wells structure

Xinxin Li(李欣欣), Zhen Deng(邓震), Yang Jiang(江洋), Chunhua Du(杜春花), Haiqiang Jia(贾海强), Wenxin Wang(王文新), and Hong Chen(陈弘)
Chin. Phys. B, 2024, 33 (**9**): 097301. DOI: 10.1088/1674-1056/ad5d99

Effect of crystallographic orientations on transport properties of methylthiol-terminated permethyloligosilane molecular junction

Ming-Lang Wang(王明郎), Bo-Han Zhang(张博涵), Wen-Fei Zhang(张雯斐), Xin-Yue Tian(田馨月), Guang-Ping Zhang(张广平), and Chuan-Kui Wang(王传奎)
Chin. Phys. B, 2022, 31 (**7**): 077303. DOI: 10.1088/1674-1056/ac4cbf

Fabrication of sulfur-doped cove-edged graphene nanoribbons on Au(111)

Huan Yang(杨欢), Yixuan Gao(高艺璇), Wenhui Niu(牛雯慧), Xiao Chang(常霄), Li Huang(黄立), Junzhi Liu(刘俊治), Yiyong Mai(麦亦勇), Xinliang Feng(冯新亮), Shixuan Du(杜世萱), and Hong-Jun Gao(高鸿钧)
Chin. Phys. B, 2021, 30 (**7**): 077306. DOI: 10.1088/1674-1056/abfbd0

Dehydrogenation-induced polarity flipping of charge carriers and conductance enhancement in nitrogen-containing heterocyclic molecule-anchored single-molecule junctions

Qi Zhou(周琦), Ruimei Liu(刘瑞梅), Guang-Ping Zhang(张广平),
Chuan-Kui Wang(王传奎)[†], and Minglang Wang(王明郎)[‡]

Shandong Key Laboratory of Medical Physics and Image Processing & Shandong Provincial Engineering and Technical Center of Light Manipulations, School of Physics and Electronics, Shandong Normal University, Jinan 250358, *China*

(Received 8 July 2025; revised manuscript received 12 September 2025; accepted manuscript online 30 September 2025)

Achieving high conductance and dual charge carriers in molecular junctions is essential for developing logical building blocks in molecular electronics. In this study, we investigated the electrical transport properties of nitrogen-containing heterocyclic molecule (N3C)-anchored single-molecule junctions using the nonequilibrium Green's function based on density functional theory. Our findings reveal that dehydrogenation is an effective strategy for achieving two charge-carrier polarities and improving conductance. In particular, dehydrogenation changed the N3C anchor from an electron-rich to an electron-deficient state, reversing the direction of charge transfer and that of the associated interfacial dipole. Consequently, electrons were replaced by holes as the primary charge carriers. Additionally, the number of removed hydrogen atoms critically governs the charge-transport behavior of molecular junctions. When the anchor groups were connected by conjugated molecular bridges, p-type and n-type molecular junctions were produced by removing three and four hydrogen atoms, respectively, significantly increasing junction conductance in both cases. These findings demonstrate that nitrogen-containing heterocyclic molecules are promising anchor groups for achieving two charge-carrier polarities and enhancing conductance through dehydrogenation.

Keywords: molecular electronics, single-molecule devices, charge carrier polarity, dehydrogenation

PACS: 73.63.–b, 31.15.at, 31.15.A–, 31.15.E

DOI: 10.1088/1674-1056/ae0d56 **CSTR:** 32038.14.CPB.ae0d56

1. Introduction

In recent years, single-molecule electronics has attracted significant attention for their potential to develop both traditional and novel functional components within physical scale limitations.[1–12] Numerous high-performance single-molecule functional components, including transistors, switches, energy-storage devices, and thermoelectric devices, have been designed and fabricated.[13–22] Complementary metal–oxide–semiconductor transistors, the cornerstone of contemporary information technology, are fabricated using silicon-based p- and n-type transistors. A critical challenge is the development of a single-molecule electronic component with both p- and n-type junctions. In general, a p-type junction, with holes as the primary charge carriers, is formed when occupied molecular orbitals act as transport channels. In contrast, an n-type junction, with electrons as the primary charge carriers, is formed when empty molecular orbitals serve as transport channels. The transport channel is determined by the molecular orbital nearest to the Fermi level (E_F).

Electrodes, core molecules, and interfaces are crucial components of molecular junctions. Experimental and theoretical studies have demonstrated that these components regulate the polarity of charge carriers to create n- and p-type junctions. The majority charge carriers in N-heterocyclic carbene-based junctions shifted from electrons to holes when Pt electrodes were used instead of Au.[23] Increasing the number of oligothiophene units also changed the charge-carrier polarity.[24] Furthermore, the charge-carrier polarity systematically shifted from holes to electrons when a family of pentamers designed to improve the electron affinity of fixed-length oligothiophenes was used.[25] In addition, a force-modulated cyclopropane ring reversibly and repeatedly changed from open to closed states, resulting in ambipolarity in the charge carriers.[26] Pyridine- and thiol-terminated molecules, commonly used as linkers to Au electrodes, have been shown to form n- and p-type junctions, respectively.[27–35] Ambipolar charge transport has also been achieved by modifying the interfacial conformation through variations in the number of covalent bonds attached to the graphene electrodes.[36] Although these approaches effectively regulate the charge-carrier polarity, they considerably alter the structure of molecular junctions, increasing the complexity of their applications. In contrast, a recently developed method involving in situ dehydrogenation can reverse the polarity of the charge carrier while inducing only minimal structural changes to the molecular junctions. In the orig-

[†]Corresponding author. E-mail: ckwang@sdnu.edu.cn
[‡]Corresponding author. E-mail: wangminglang@sdnu.edu.cn

© 2026 Chinese Physical Society and IOP Publishing Ltd. All rights, including for text and data mining, AI training, and similar technologies, are reserved.

inal report of this method, dehydrogenation improved the low-bias conductance and changed the polarity of charge carriers in imidazole-linked molecular junctions.[37] In addition, we recently discovered that dehydrogenation of azaindole-based molecular junctions switched the polarity of charge carriers and significantly enhanced the conductance by achieving resonance transmission at E_F.[38] However, the scope of its application is limited by the extremely low conductance before dehydrogenation and the significant conductance difference following dehydrogenation. Achieving considerable conductance in n- and p-type junctions requires extensive research to determine the effect of dehydrogenation on the transmission properties of molecular junctions.

In this study, we examined the transport properties of nitrogen-containing heterocyclic molecule $N_3C_6H_5$(N3C)-anchored single-molecule junctions using the density functional theory (DFT)-based nonequilibrium Green's function method. We systematically investigated the influence of stepwise hydrogen abstraction on the electronic transport properties of N3C-anchored single-molecule junctions. This study aims to provide a mechanistic understanding of interfacial electronic interactions in response to chemical modifications and to establish a controllable framework for engineering high-performance molecular junctions.

2. Calculation method

In this study, Atomistix ToolKit (ATK) software was used to calculate electronic structures and optimize molecules and molecular junctions. ATK is a powerful platform for implementing DFT calculations.[39–44] Troullier–Martins pseudopotentials were used to define the atomic cores, and a finite-range numerical orbital basis set was used to expand the valence electron orbitals.[45–48] In this study, elements, including C, H, N, S, F, and Au, built into molecules and molecular junctions were described using the double-zeta plus polarization basis set. The exchange–correlation functional was the generalized gradient approximation devised by Perdew, Burke, and Ernzerhof.[49,50] The cutoff energy for drawing real-space grids was 400.0 Ry. The geometry was optimized using the conventional conjugate gradient method until the residual forces were reduced to less than 0.02 eV/Å.

The transport properties of the molecular junctions were calculated using ATK by implementing the nonequilibrium Green's function method based on DFT.[51–54] The supercell included adatomic Au surfaces and Au(111) atomic layers arranged in a (4×4) plane. The pseudopotentials, basis set, and exchange–correlation functional were identical to those used in the above DFT calculations. Periodic boundary conditions were used to simulate infinite electrodes on the plane transverse to the transport direction. The electronic density was calculated using Green's function, which was evaluated using eight points along a line in the complex plane, 30 energy points along a semicircle, and eight poles for the Fermi function at 300 K. The transmission coefficient $(T(E))$ of the molecular junctions was calculated as follows:[55]

$$T(E) = \frac{1}{\Omega_{2\mathrm{DBZ}}} \int_{2\mathrm{DBZ}} \mathrm{Tr}[\Gamma_{\mathrm{L}\sigma} G^{\mathrm{R}}_{\sigma} \Gamma_{\mathrm{R}\sigma} G^{\mathrm{R}\dagger}_{\sigma}] \mathrm{d}\boldsymbol{k},$$

where σ represents the spin, $\Omega_{2\mathrm{DBZ}}$ indicates the area of the two-dimensional (2D) Brillouin zone, $\Gamma_{\mathrm{R/L}\sigma}$ represents the interfacial coupling, and G^{R}_{σ} $(G^{\mathrm{R}\dagger}_{\sigma})$ signifies the retarded (advanced) Green's function.

3. Results and discussion

Models for a family of molecular junctions were constructed using N3C as the anchoring group to connect the electrodes. Figure 1(a) illustrates the chemical structures with various bridge groups, denoted as N3C1–N3C3. The terminal C atom of the five-membered ring of N3C is bonded to the Au adatom on the Au surface to create molecular junctions. Figure 1(b) illustrates the optimal molecular junctions utilizing N3C1 before (top panel) and after (lower panel) dehydrogenation. In the optimized atomic structures, the yellow, gray, blue, and white spheres represent gold, carbon, nitrogen, and hydrogen atoms, respectively. Au–N3C1(N3C1dH)–Au represents the situation before (after) dehydrogenation. The optimized Au–C bond lengths of the two junctions in Fig. 1(b) are nearly identical, measuring 2.02 Å and 2.04 Å, respectively, suggesting that the interfacial contact between Au and C remains constant, regardless of the dehydrogenation state. The N3C2 and N3C3 molecular junctions exhibit comparable results with Au–C bonds of almost identical length (see Fig. S1 in the supporting information).

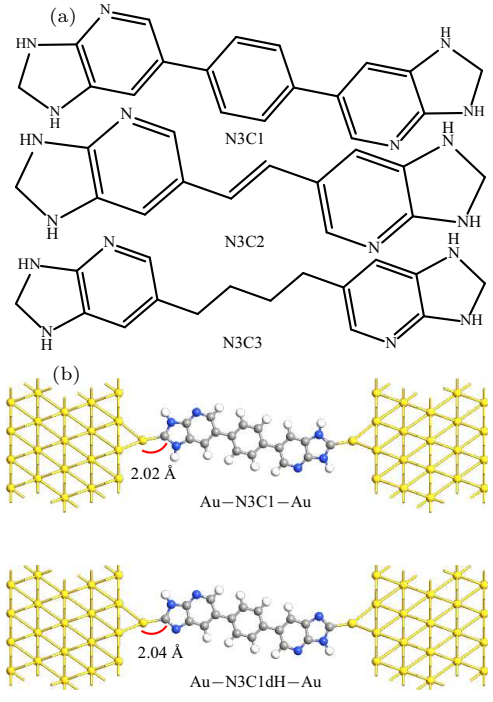


Fig. 1. Chemical structures of nitrogen-containing heterocyclic molecule $N_3C_6H_5$(N3C)-anchored molecules N3C1–N3C3 (a). Optimized atomic structures of Au–N3C1(dH)–Au (b).

Notably, the bond lengths associated with the terminal C atom change from approximately 1.37 Å and 1.37 Å before dehydrogenation to 1.39 Å and 1.32 Å following dehydrogenation, whereas the other bond length remains unchanged (see Fig. S2). The interfacial electronic structure, a critical factor in regulating charge carrier polarity, is significantly dependent on the modified bond length, as shown in previous studies.[37,38,56] Therefore, investigating the effect of dehydrogenation on the primary charge carriers is essential.

The transmission spectra of Au–N3C*n*(N3C*n*dH)Au (n = 1, 2, and 3) were calculated (Fig. 2). To analyze the charge carrier type, the frontier molecular orbitals (FMOs) of isolated N3C*n*, the transmission eigenchannel at E_F, and molecular projected self-consistent Hamiltonian states (MPSHs) of the molecular junctions were studied (Fig. 2). Dehydrogenation causes an upward shift in the FMOs of N3C1, changing HOMO-2, HOMO-1, HOMO, and LUMO to HOMO-1, HOMO, LUMO, and LUMO+1, respectively. However, the conductance orbitals nearest the E_F of the electrode in the molecular junctions are FMOs with superior delocalization characteristics: HOMO-2 and LUMO before dehydrogenation, and HOMO-1 and LUMO+1 after dehydrogenation. This behavior could be attributed to the π-bridged electronic states in these delocalized FMOs, which enhance coupling between the interfacial anchors. In contrast, the interactions between the left and right anchors are weak in HOMO-1 and HOMO of N3C1 and HOMO and LUMO of N3C1dH owing to the absence of electronic state distribution between the anchors. When bonded to the electrodes, molecules with stronger interfacial coupling tend to form stable junctions.[57,58] Analysis of the FMOs and MPSHs reveals that HOMO-2 and LUMO dominate two prominent transmission peaks at −2.62 eV and 0.12 eV, respectively, in Au–N3C1–Au. The LUMO tail dominates $T(E)$ at E_F ($T(E_F)$), suggesting that this junction is n-type (with electrons as the primary charge carriers). This finding is further supported by the comparable morphology of the LUMO of isolated N3C1, the eigenchannel at E_F, and the MPSHs. The $T(E_F)$ is 5.63×10^{-2} (Table 1), which is proportional to the conductance in the linear response approximation.[55] After dehydrogenation, the $T(E)$ spectra of the Au–N3C1dH–Au molecular junction move upward, resulting in a peak at −0.12 eV dominated by HOMO-1 and a peak at 2.74 eV dominated by LUMO+1. HOMO-1 is closer to E_F, and its tail contributes to $T(E_F)$. The primary charge carriers switch to holes, forming a p-type junction, as further verified by the transport channel at E_F, which is identical to that of HOMO-1. The $T(E_F)$ of Au–N3C1dH–Au decreases to 8.77×10^{-3} owing to a weaker interfacial interaction (indicated by a narrower peak width), although the principal transmission peaks before and after dehydrogenation exhibit a similar energy separation of 0.12 eV to E_F. Therefore, the charge carriers switch from electrons to holes upon dehydrogenation.

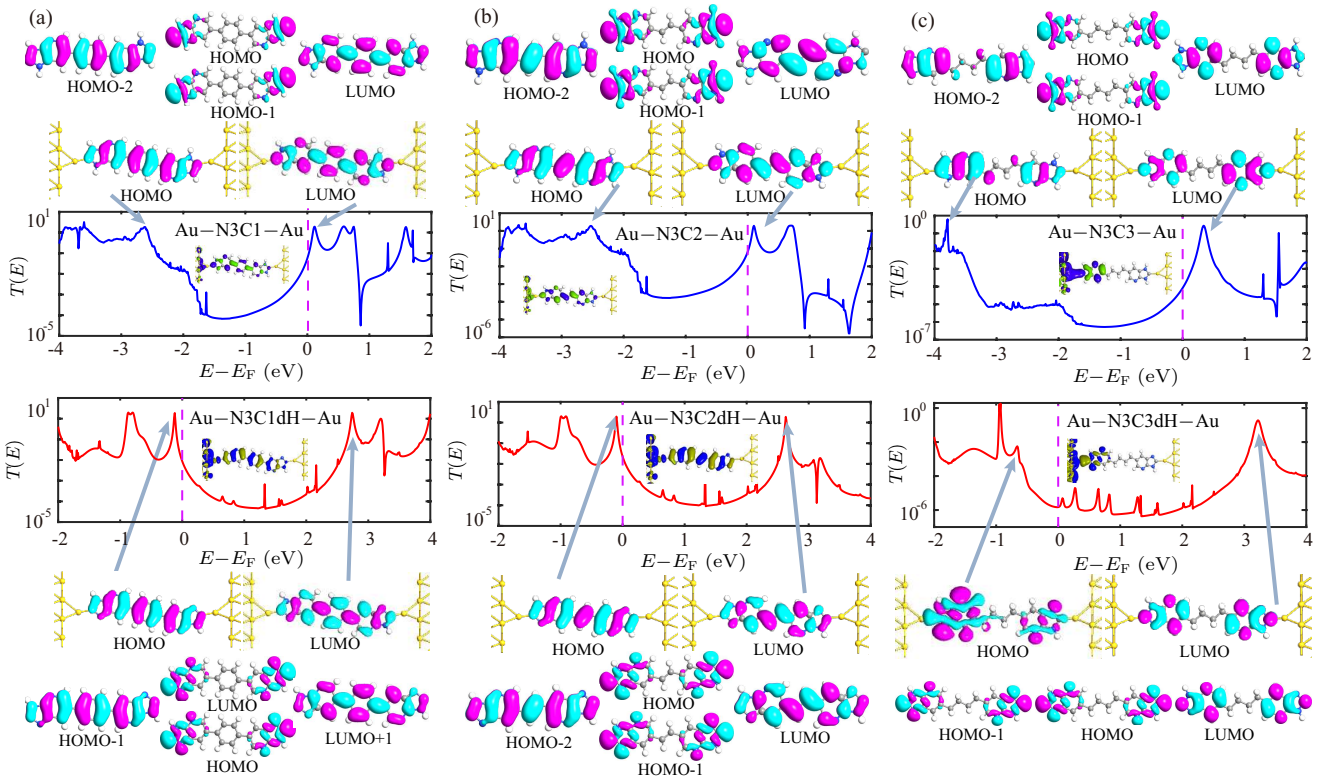


Fig. 2. Molecular orbitals of isolated N3C1 (a), N3C2 (b), and N3C3 (c) with equilibrium transmission spectra, MPSHs, and eigenchannels at E_F obtained for Au–N3C1–3(dH)–Au.

Table 1. Transmission coefficient at E_F, charge transfer amount between electrodes and molecules, and interfacial dipoles calculated at the left and right molecule–electrode interfaces for Au–N3C1–3(dH)–Au.

Junction	Au–N3C1–Au	Au–N3C1dH–Au	Au–N3C2–Au	Au–N3C2dH–Au	Au–N3C3–Au	Au-M3C3dH–Au
$T(E_F)$	5.63×10^{-2}	8.77×10^{-3}	6.65×10^{-2}	2.25×10^{-2}	8.31×10^{-5}	1.48×10^{-6}
Q/e$^-$	–0.43	0.40	–0.41	0.39	–0.46	0.42
μ_L/D	2.56	–3.81	2.51	–2.89	3.29	–2.99
μ_R/D	2.63	–3.80	2.58	–2.94	3.36	–3.06

In contrast to N3C1, the morphologies of the FMOs of N3C2 are unaffected by dehydrogenation. However, in Au–N3C2–Au, HOMO-2 dominates the transmission peak at −2.53 eV, and the LUMO dominates the peak at 0.1 eV. Therefore, the primary charge carriers are electrons because the LUMO dominates the $T(E_F)$, as confirmed by the identical morphology of the LUMO and the eigenchannel at E_F. Following dehydrogenation, the origin of the two transmission peaks nearest E_F is identical to that observed before dehydrogenation. However, the $T(E)$ spectra shift upward, bringing the HOMO-2-dominated transmission peak closer to E_F (−0.1 eV) than the LUMO-dominated peak (2.63 eV). Consequently, holes become the primary charge carriers, as indicated by the similar morphology between HOMO-2 and the eigenchannel at E_F (Fig. 2(b)). The change in the $T(E_F)$ owing to dehydrogenation is relatively small, decreasing from 6.65×10^{-2} to 2.25×10^{-2}. Achieving similar $T(E)$ values at both junctions may produce a practical p–n junction.

Unlike N3C2, dehydrogenation of N3C3 has a substantial impact on its electrical structure, where the HOMO and HOMO-1 levels undergo significant changes (Fig. 2(c)). Following electrode attachment, the HOMO-2 and LUMO of the isolated N3C3 become the molecular orbitals closest to E_F. Following dehydrogenation, neither the HOMO nor LUMO change after electrode attachment. Moreover, in Au–N3C3–Au, the LUMO dominates the $T(E_F)$, whereas in Au–N3C3dH–Au, the HOMO is dominant. This finding was further corroborated by the eigenchannel at E_F for both molecular junctions, which indicates that electrons and holes are the primary charge carriers in Au–N3C3–Au and Au–N3C3dH–Au, respectively. The $T(E_F)$ values are extremely small, 8.31×10^{-5} for Au–N3C3–Au and 1.48×10^{-6} for Au–N3C3dH–Au. This reduction in $T(E)$ is attributed to the alkyl bridge, which reduces the contact between the two anchoring groups and shifts the transmission peak away from E_F. Fig. S3 displays the computed densities of states (DOS), which are associated with the transmission spectra. The discovered transmission peaks were the result of specific electrical states. Notably, dehydrogenation changes the polarity of the charge carriers for all studied molecular junctions. The primary charge carriers shift from electrons to holes, as shown by the change in the conducting orbital from the LUMO to the HOMO (HOMO-1 and HOMO-2). Consequently, N3C may be used as an anchor in molecular electronics to regulate charge-carrier polarity.

In molecular junctions, the interface is a crucial factor that influences transport properties. As key components of the interface, anchor groups may affect interfacial coupling by controlling interfacial charge transfer, which can shift and broaden the molecular level. The physical mechanism underlying the shift in the charge-carrier polarity induced by dehydrogenation was evaluated by charge-transfer analysis. The molecular junction was divided into three sections: the molecular core, both electrodes, and the complete junction. The plane-averaged electron density difference ($\delta\rho$) among the three sections was calculated as follows:

$$\delta\rho = \rho_c - \rho_m - \rho_e,$$

where ρ_c, ρ_m, and ρ_e are the electron densities of the complete junction, molecular core, and electrodes, respectively. The charge-transfer quantity (Q) is defined as follows:

$$Q = \int \delta\rho \, dz.$$

The $\delta\rho$ along the z-direction of Au–N3C1(dH)–Au was calculated (Fig. 3). The $\delta\rho$ before and after dehydrogenation is represented by the blue and red lines, respectively. In molecular junctions, a zone with $\delta\rho$ larger than zero indicates that electrons have been acquired, whereas a zone with $\delta\rho$ smaller than zero indicates that electrons have been lost. Significant variations in $\delta\rho$ were observed near the contact, with noticeable peaks and dips. Specifically, the peaks show the majority of electrons being accumulated, while the dips show the majority of electrons being lost. Consequently, in Au–N3C1–Au, the electrons move from the molecule to the electrodes (denoted by a negative sign), whereas in Au–N3C1dH–Au, the reverse trend is observed (denoted by a positive sign), giving charge-transfer numbers of approximately −0.43 and 0.40, respectively. The values are summarized in Table 1. The molecular junctions constructed using N3C2 and N3C3 represented the same scenario. Au–N3C2–Au (Au–N3C3–Au) junctions exhibit molecule-to-electrode charge transfer with charge-transfer numbers of −0.41 (−0.46), which changes to electrode-to-molecule charge transfer upon dehydrogenation with charge-transfer numbers of 0.39 (0.42) for Au–N3C2dH–Au (Au–N3C3dH–Au), as shown in Figs. S4 and S5 and Table 1. Overall, dehydrogenated N3C (N3CdH) acts as an electron acceptor, accepting electrons from the electrodes, whereas the N3C anchors act as electron donors, transferring electrons

to the electrodes. Dehydrogenation functions as a switch, changing an electron-rich state to an electron-deficient state, which can raise the molecular levels, as confirmed by Hou *et al.*[37] Consequently, the conductance orbital below E_F is closer to E_F than that above E_F, indicating that the charge carriers are converted from electrons to holes.

Furthermore, the interfacial dipoles affect the molecular level. In general, interfacial dipoles pointing toward the electrodes facilitate HOMO occupancy, whereas those pointing in the opposite direction support LUMO occupation. To validate the previous results, the local dipole at the interface (P) is calculated as follows:

$$P = \int_0^C -z \times \delta\rho \, \mathrm{d}z,$$

where z is the coordinate relative to the coordinate of the Au adatom (point 0), and C is the midpoint between the left and right adatom Au atoms, which serves as the approximate molecular center. Both interfacial dipoles are directed toward molecules, with strengths of 2.56 D and 2.63 D, demonstrating an asymmetric junction before dehydrogenation for Au–N3C1–Au (Fig. 3(a)).

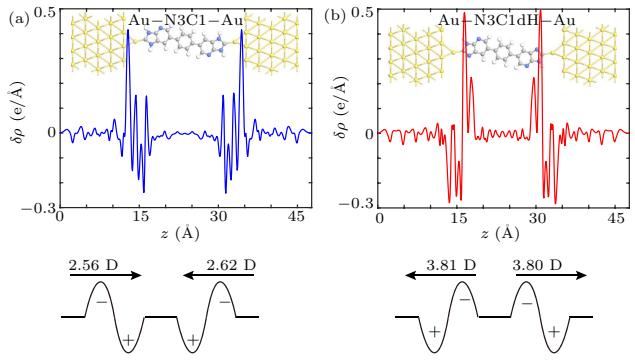


Fig. 3. Plane-averaged electron density differences of Au–N3C1–Au (a) and Au–N3C1dH–Au (b) and corresponding schematics of interfacial dipoles induced by charge transfer.

Conversely, the interfacial dipoles of the dehydrogenated junction in Fig. 3(b) illustrate the opposite orientation and point to the electrodes with strengths of 3.81 D and 3.80 D. Therefore, the reversal of the dipole direction upon dehydrogenation promotes HOMO occupation rather than LUMO occupation, which confirms that dehydrogenation caused the charge-carrier polarity to switch by affecting the interfacial structures. A positive sign indicates an orientation toward the molecules, whereas a negative sign indicates the opposite orientation. The interfacial dipole strengths of Au–N3C2–Au and Au–N3C3–Au are summarized in Table 1 and exhibit an identical pattern to that of Au–N3C1–Au. Before dehydrogenation, interfacial dipoles, with strengths of 2.51 D/2.58 D and 3.29 D/3.36 D for Au–N3C2–Au and Au–N3C3–Au, respectively, pointed away from the electrodes toward the molecules, and the direction reversed upon dehydrogenation, with strengths of −2.89 D/ − 2.94 D and −2.99 D/ − 3.06 D for Au–N3C2dH–Au and Au–N3C3dH–Au, respectively (see Figs. S4 and S5). These findings indicate that carrier exchange occurs when the interfacial dipole moment is reversed.

To confirm that the change in charge-carrier polarity originates specifically from the dehydrogenated hydrogen atoms, a model of Au–N3C2S–Au was built by substituting the S atom for the unremoved hydrogen N atom in the terminal group, as shown in the inset of Fig. 4(a). The yellow, gray, blue, bright yellow, and white spheres represent the gold, carbon, nitrogen, sulfur, and hydrogen atoms, respectively. The dehydrogenated junction is denoted as Au–N3C2SdH–Au (Fig. 4(b)).

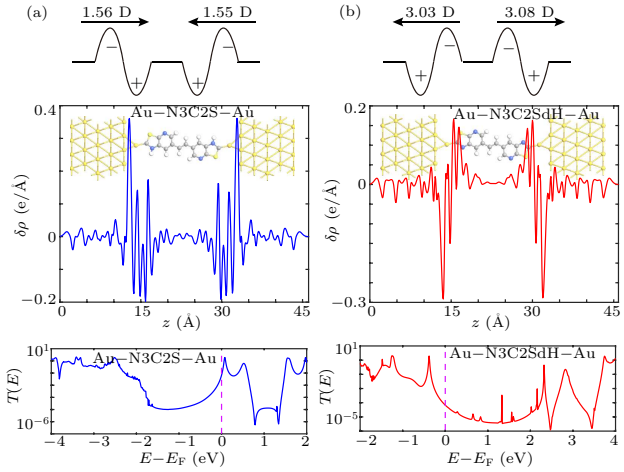


Fig. 4. Schematic diagram of interfacial dipoles induced by charge transfer, plane-averaged electron density difference, and equilibrium transmission spectra of Au–N3C2S–Au (a) and Au–N3C2SdH–Au (b).

As illustrated in Figs. 4(a) and 4(b), charge transfer primarily takes place at the interfaces, as seen by the apparent peaks and valleys. Quantitatively, Au–N3C2S–Au showed a charge-transfer number of 0.31, with electron transfer from the molecule to the electrodes, resulting in interfacial dipoles pointing from the electrodes to the molecule. The dipole strengths at the left and right interfaces are approximately 1.56 D and 1.55 D, respectively. Conversely, Au–N3C2SdH–Au exhibits the opposite behavior, with electrons (approximately 0.43) moving from the electrodes to the molecule, resulting in interfacial dipoles pointing from the molecule to the electrodes, with strengths of approximately 3.03 D and 3.08 D at the left and right interfaces, respectively. According to previous results, we can infer that Au–N3C2S–Au is an n-type junction with electrons as the primary charge carriers, and Au–N3C2SdH–Au is a p-type junction with holes as the primary charge carriers. Au–N3C2S–Au's n-type junction is confirmed by the transmission peak closest to E_F in the $T(E)$ spectra being above E_F, while Au–N3C2SdH–Au's p-type junction is confirmed by the transmission peak closest to E_F being below E_F (Fig. 4). Therefore, these results confirm the validity of the proposed mechanism, in which dehydrogenation is the primary cause of the switching between carrier types. Furthermore, an F atom labeled by a green sphere in the optimized

structures was substituted for the hydrogen atom at the dehydrogenation site. The results show that the $T(E)$ spectra resemble those of the junctions before dehydrogenation (see Fig. S6). Therefore, electrons remain the primary charge carriers, further confirming that the polarity change of the charge carriers originates from the dehydrogenation process.

According to previous reports, dehydrogenation enhanced the conductivity in addition to switching the carrier type.[37,38] However, dehydrogenation reduced the conductance of the molecular junctions considered in this study when N3C was used as an anchor group attached to the electrodes. Previous research demonstrated that the number of removed hydrogen atoms influences the junction conductance.[38] The removal of one, two, three, and four hydrogen atoms from the terminal group was compared (see Fig. S7). Removing one hydrogen atom did not improve the junction conductance in any of the studied systems; however, removing three or four hydrogen atoms significantly increases the junction conductance. The $T(E)$ spectra of N3C1 and N3C2, in which three (N3C*n*d3H) and four (N3C*n*d4H) hydrogen atoms are eliminated, respectively, are shown in Fig. 5.

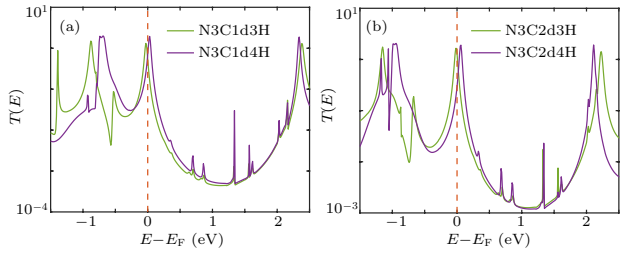


Fig. 5. Equilibrium transmission spectra of N3C1 (a) and N3C2 (b) after removing three (N3C*n*d3H) and four (N3C*n*d4H) hydrogen atoms.

Despite the high conductance of these molecular junctions, their conductance mechanisms were distinct. When three hydrogen atoms were removed from N3C1, the peak at −0.03 eV (nearest E_F) indicates that holes are the primary charge carriers with a $T(E_F)$ of approximately 0.53. Conversely, the peak at 0.03 eV is closer to E_F when four hydrogen atoms are removed (N3C1d4H), resulting in an n-type junction with a $T(E_F)$ of approximately 0.69. N3C2 exhibits a comparable scenario to the N3C1 system. The primary conductive channel of N3C2d3H is located at −0.02 eV, resulting in a p-type junction with a large $T(E_F)$ of approximately 1.28. The primary conductive channel of N3C2d4H is located at 0.06 eV, resulting in an n-type junction with a $T(E_F)$ of approximately 0.29. In addition, we computed the transmission properties of the dehydrogenated Au–N3C1dH–Au junction, as an example, for different positions of the anchors and removed hydrogen atoms (see Fig. S8). The findings indicate that the $T(E_F)$ is influenced by the dehydrogenation position. In order to remove three hydrogen atoms, two hydrogen atoms are removed from one terminal group and one hydrogen atom is removed from the other group. When a hydrogen atom located next to the six-membered ring's nitrogen atom is removed, $T(E_F)$ is higher. In contrast, the charge carrier polarity is unaffected by the dehydrogenation position. Therefore, when N3C is used as the anchor group, carrier-polarity switching and high conductance were achieved by removing different numbers of hydrogen atoms.

4. Conclusions

A quantum transport approach was used to investigate the transport properties of a series of N3C-anchored molecular junctions. The findings revealed that transmission across the molecular junctions is considerably influenced by dehydrogenation. In particular, dehydrogenation caused the N3C anchor to transition from an electron-rich to an electron-deficient state, changing the direction of the interfacial electron transfer from electrodes to molecules, which further reversed the interfacial dipolar direction. Consequently, n- and p-type molecular junctions were obtained. Furthermore, the number of hydrogen atoms removed from the N3C anchor influences the intrinsic mechanism and magnitude of the conductance of the molecular junction. In particular, when three and four hydrogen atoms were removed from N3C1 and N3C2, respectively, the conductance is significantly enhanced. However, the molecular junctions with three hydrogen atoms removed (N3C1d3H and N3C2d3H) exhibited p-type behavior, with holes as the primary charge carriers. In contrast, N3C1d4H and N3C2d4H, with four hydrogen atoms removed, form n-type molecular junctions with electrons as primary charge carriers. Dehydrogenation can switch the polarity of the charge carriers in molecular junctions comprising N3C as an anchor. Moreover, the conductance magnitude of the molecular junctions can be increased by precisely controlling the number of removed hydrogen atoms. These results highlight the potential of N3C for molecular electronics applications. These insights demonstrate the dual modulation of the charge-carrier type and conductance via dehydrogenation and pave the way for future design strategies in molecular-scale transistors and logic elements.

Acknowledgement

Project supported by the National Natural Science Foundation of China (Grants Nos. 12304316 and 22173052).

References

[1] Chen L, Feng A, Wang M, Liu J, Hong W and Xiang D 2018 *Sci. China Chem.* **61** 1368
[2] Evers F, Korytár R, Tewari S and van Ruitenbeek J M 2020 *Rev. Mod. Phys.* **92** 035001
[3] Shiri M, Zhang H and Wang K 2024 *ACS Appl. Electron. Mater.* **6** 8626
[4] Deng J, González M T, Zhu H, Anderson H L and Leary E 2024 *J. Am. Chem. Soc.* **146** 3651
[5] Zhang H, Li J, Yang C and Guo X 2024 *Acc. Mater. Res.* **5** 971

[6] Yan C, Fang C, Gan J, Wang J, Zhao X, Wang X, Li J, Zhang Y, Liu H, Li X, Bai J, Liu J and Hong W 2024 *ACS Nano* **18** 28531
[7] Li T, Bandari V. K and Schmidt O. G 2023 *Adv. Mater.* **35** 2209088
[8] Dief E. M, Low P. J, Díez-Pérez I and Darwish N 2023 *Nat. Chem.* **15** 600
[9] Hu S, Zhang G and Zhang B 2025 *Chin. Phys. B* **34** 068903
[10] Tian Y, Zheng Q, Zhao J 2023 *Chin. Phys. Lett.* **40** 126301
[11] Hu Y, Li X, Li Q and Yang J 2022 *Angew. Chem. Int. Edit.* **61** e202205036
[12] Jia C, Li X, Li Q and Yang J 2023 *Phys. Rev. B* **107** L140404
[13] Jiang T, Zeng B, Zhang B and Tang L 2023 *Chem. Soc. Rev.* **52** 5968
[14] Duggin M, Bissember A C and Fuller R O 2025 *Chem. Asian J.* **20** e202401550
[15] Huang Y, He G, Huang G, Wang M, Li Y, Yang F, Gao C and Wang L 2025 *J. Colloid Interf. Sci.* **689** 137256
[16] Chen L, Yang Z, Lin Q, Li X, Bai J and Hong W 2024 *Langmuir* **40** 1988
[17] Zhang Y, Qiu R, Qu K, Zhang C, Stoddart J F and Chen H 2024 *Sci. Chin. Mater.* **67** 709
[18] Li H, Liu J, Geng B, Qiu S, Chen Z, Yang Y and Zhang Q 2025 *Chem. Asian J.* **20** e202401774
[19] Huang Y, He G, Huang G, Wang M, Li Y, Yang F, Gao C and Wang L 2025 *J. Colloid Interf. Sci.* **689** 137256
[20] Wang D, Xu W, Hu Y, Wang T, Moloney M. G and Du W 2025 *ACS Appl. Mater. Interfaces* **17** 12875
[21] Zhang M, Yang Z, Li S and Mu Y 2025 *J. Mater. Chem. C* **13** 4557
[22] Pareek A, Mehboob M, Cieplak M, Majdecki M, Szabat H, Noworyta K, Połczyński P, Morawiak M, Sharma P, Foroutan-Nejad C and Gawel P 2025 *J. Am. Chem. Soc.* **147** 5996
[23] Wang M and Wang C 2020 *Chin. Phys. B* **29** 113101
[24] Dell E. J, Capozzi B, Xia J, Venkataraman L and Campos L M 2015 *Nat. Chem.* **7** 209
[25] Low J. Z, Capozzi B, Cui J, Wei S, Venkataraman L and Campos L M 2017 *Chem. Sci.* **8** 3254
[26] Shao J, Zhang X, Chen Y and Zheng Y 2016 *Npj Comput. Mater.* **2** 2
[27] Tan A, Balachandran J, Sadat S, Gavini V, Dunietz B. D, Jang S and Reddy P 2011 *J. Am. Chem. Soc.* **133** 8838
[28] de Melo Souza A, Rungger I, Pontes R. B, Rocha A. R, da Silva A. J. R, Schwingenschlöegl U and Sanvito S 2014 *Nanoscale* **6** 14495
[29] Su T. A, Neupane M, Steigerwald M. L, Venkataraman L and Nuckolls C 2016 *Nat. Rev. Mater.* **1** 16002
[30] Wang M, Wang H, Zhang G, Wang Y, Sanvito S and Hou S 2018 *J. Chem. Phys.* **148** 184703
[31] Garner M. H, Li H, Neupane M, Zou Q, Liu T, Su T. A, Shangguan Z, Paley D. W, Ng F, Xiao Nuckolls S. C, Venkataraman L and Solomon G C 2019 *J. Am. Chem. Soc.* **141** 15471
[32] Song X, Song K Y and Zang Y 2022 *Sci. Sin. Chim.* **52** 181
[33] Zhang C, Cheng J, Wu Q, Hou S, Feng S, Jiang B, Lambert C. L, Gao X, Li Y and Li J 2023 *J. Am. Chem. Soc.* **145** 1617
[34] Liu H, Zhang H, Zhao Y, Liu J and Hong W 2023 *Trend Chem.* **5** 367
[35] Li Y, Tang A, Wang R, Li Y, Ma C and Li H 2023 *Chem. Commun.* **59** 4628
[36] Jiang Z, Wang H, Wang Y, Sanvito S and Hou S 2017 *J. Phys. Chem. C* **121** 27344
[37] Li S, Jiang Y, Wang Y, Sanvito S and Hou S 2021 *J. Phys. Chem. Lett.* **12** 7596
[38] Wang M, Zhou Q, Xu Z and Zhang G 2024 *J. Phys. Chem. A* **128** 9861
[39] Atomistix toolKit version 2018.06 synopsys quantumwise A/S (www.quantumwise.com)
[40] Smidstrup S, Markussen T, Vancraeyveld P, Wellendorff J, Schneider J, Gunst T, Verstichel B, Stradi D, Khomyakov P. A, Vej-Hansen U. G, Lee M, Chill S, Rasmussen F, Penazzi G, Corsetti F, Ojanperä A, Jensen K, Palsgaard M, Martinez U, Blom A, Brandbyge M and Stokbro K 2020 *J. Phys.: Condens. Matter* **32** 015901
[41] Hou L, Liu R, Yuan H, Kong D, Shen W, Zang J, Guo J, Dai S, Wang M, Xu T, Li X and Wang Y 2021 *Rare Metals* **40** 1391
[42] Wang M, Zhang W and Tian X 2022 *Phys. E* **140** 115224
[43] Zhang W, Zhang G, Li Z, Fu X, Wang C and Wang M 2022 *Phys. Chem. Chem. Phys.* **24** 1849
[44] Kong D, Wang Y, Huang S, Lim Y, Wang M, Xu T, Zang J, Li X and Yang H 2022 *J. Colloid. Interf. Sci.* **607** 1876
[45] Troullier N and Martins J L 1991 *Phys. Rev. B* **43** 1993
[46] Soler J M, Artacho E, Gale J D, García A, Junquera J, Ordejón P and Sánchez-Portal D 2002 *J. Phys.: Condens. Matter* **14** 2745
[47] García-Gil S, García A, Lorente N and Ordejón P 2009 *Phys. Rev. B* **79** 075441
[48] Tian X, Zhang W, Zhang G, Li Z, Wang C and Wang M 2023 *Phys. Chem. Chem. Phys.* **25** 11545
[49] Perdew J. P, Burke K and Ernzerhof M 1996 *Phys. Rev. Lett.* **77** 3865
[50] Wang M, Chen X, Lu W, Tian X and Zhang G 2023 *Phys. Chem. Chem. Phys.* **25** 13673
[51] Brandbyge M, Mozos J, Ordejón P, Taylor J and Stokbro K 2002 *Phys. Rev. B* **65** 165401
[52] Wang S, Kong Y, Zhang S, Wang. M, Wei M, Wang C and Zhang G 2024 *ACS Appl. Mater. Interfaces* **16** 55813
[53] Yao L, Yun J, Kang P, Zhao H, Yan J, Zhao W and Zhang Z 2024 *Appl. Surf. Sci.* **652** 159363
[54] Yang C, Chen Z, Yu C, Cao J, Ke G, Zhu W, Liang W, Huang J, Cai W, Saha C, Sabuj M, Rai N, Li X, Yang J, Li Y, Huang F and Guo X 2024 *Nat. Nanotechnol.* **19** 978
[55] Datta S 1995 *Electronic transport in mesoscopic systems* (Cambridge: University Press)
[56] Wang M and Zhang G 2024 *Phys. Chem. Chem. Phys.* **26** 9051
[57] Wang M, Wang Y, Sanvito S and Hou S 2017 *J. Chem. Phys.* **147** 054702
[58] Lin J, Lv Y, Song K, Song X, Zang H, Du P, Zang Y and Zhu D 2023 *Nat. Commun.* **14** 293